ACS APPLIED MATERIALS & INTERFACES

Research Article

www.acsami.org

# Insight into the Aging Effect on Enhancement of Hydrogen-Sensing Characteristics of a Zirconia-Based Sensor Utilizing a Zn–Ta–O-Based Sensing Electrode

Sri Ayu Anggraini,[†] Michael Breedon,[‡,§] Hiroshi Ikeda,[⊥] and Norio Miura*[,⊥]

[†]Interdisciplinary Graduate School of Engineering Sciences and [⊥]Art, Science and Technology Center for Cooperative Research (KASTEC), Kyushu University, Kasuga-shi, Fukuoka 816-8580, Japan

[‡]Materials Science and Engineering Division, CSIRO, Gate 5, Normanby Road, Clayton, Victoria 3168, Australia

**ABSTRACT:** A significant enhancement in the hydrogen ($H_2$) sensitivity as well as selectivity after aging for more than 40 days has been observed for a mixed-potential-type sensor using ZnO (+84 wt % $Ta_2O_5$) as the sensing electrode (SE) and yttria-stabilized zirconia (YSZ) as the solid electrolyte. The effect of the aging process in enhancing the sensing characteristics of the sensor using ZnO (+84 wt % $Ta_2O_5$)-SE was studied here by investigating the changes in the morphology, crystal structure, chemical surface state, and catalytic properties of the SE material before and after aging at 500 °C for 80 days. X-ray diffraction measurements confirmed that the crystal structure of the SE material was found to be unaffected by aging, while the morphological change observed via scanning electron microscopy imaging indicated a decrease in the porosity and an increase in the particle size after aging. A significant change, particularly in the binding energy of Ta 4f, was also observed for the SE material after long-term aging. Although the catalytic activities toward the anodic reaction of $H_2$ and the other examined gases were moderately stable after aging, a significant decrease in the heterogeneous catalytic activity of the gas-phase reaction (oxidation) of $H_2$ was observed. Such a trend presumably resulted in a higher fraction of $H_2$ reaching the triple-phase boundary, where the electrochemical reactions generate a sensing signal (mixed potential), resulting in high $H_2$ sensitivity as well as high $H_2$ selectivity after long-term aging of the present sensor.

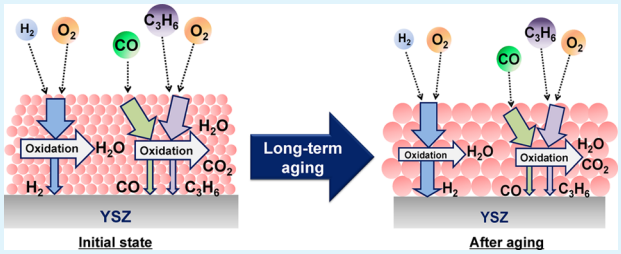


**KEYWORDS:** *hydrogen, gas sensor, aging, mixed potential, YSZ, ZnO, $Ta_2O_5$*

## 1. INTRODUCTION

Ever since hydrogen ($H_2$) was championed as a plausible and meaningful alternative energy solution with aspirations of replacing dominant fossil-fuel sources, extensive efforts have been devoted to developing a safe infrastructure to support the wider use of $H_2$ as an alternative fuel. However, the widespread use of $H_2$ raises safety concerns. Potential hazardous or lethal events can be prevented by employing a sensing device that could monitor an $H_2$ leakage or an accumulated $H_2$ concentration in facilities and vehicles that utilize $H_2$ as an energy source.

After the commercial success of an $O_2$ sensor for automotive application in 1970s,[1,2] yttria-stabilized zirconia (YSZ)-based sensors are a particularly attractive type of sensor because of their robust nature, simple support electronics required for sensing-signal interpretation, and long-term durability of sensing performances.[3,4] For mixed-potential-type YSZ-based sensors, the sensing performances will be predominantly determined by the type of sensing electrode (SE) material, the fabrication processes, and the operating conditions.[5−7] The generated sensing signal (electromotive force, emf) is governed by electrochemical reactions, involving each of oxygen and a target gas, that take place simultaneously at the interface between SE and YSZ solid electrolyte.[8−10]

Most commonly, mixed-potential theory can be rationalized by means of polarization ($I$–$V$) curves, where the intercept point of the anodic and cathodic curves mostly corresponds to the steady state of the cathodic reaction of $O_2$ and the anodic reaction of a target gas; hence, the potential at the intersect point is assigned as the "mixed potential".[11−14] Because the gas sensitivity will be largely determined by the catalytic activities of the electrode material toward heterogeneous gas-phase reactions as well as electrochemical reactions,[15−17] searching for a suitable SE material is one of the most important aspects in developing a high-performance mixed-potential-type YSZ-based gas sensor. The catalytic activity of an electrode material can be controlled by factors such as the morphology, crystal structure, or even operating conditions.[18−20] Consequently, controlling the catalytic activity of the electrode material is also a highly desirable attribute in the field of gas-sensor engineering. At the same time, the aging process is a challenge

Received: September 12, 2013
Accepted: October 21, 2013
Published: October 21, 2013

  

that is often faced in sensor development and sometimes plays a role in changing the sensing properties of an electrode material. Therefore, any insight into how and why an aging process affects the sensing properties of an electrode material is very useful and particularly important for those who are working in the field of gas-sensor research.

Previously, we have proposed that Zn−Ta−O-based oxides can be used as an $H_2$-sensitive SE material for a mixed-potential-type YSZ-based sensor.[21] Especially, the addition of 84 wt % $Ta_2O_5$ into ZnO was reported to give a sensitive and relatively selective response toward $H_2$.[21] After 40 days of aging at 500 °C, the sensitivity of the sensor toward 400 ppm $H_2$ had peaked and stabilized at around −800 mV.[22] Interestingly, this significant enhancement in the $H_2$ sensitivity after long-term aging was not accompanied by an increase in sensitivity toward other examined gases such as CO and $C_3H_6$. Thus, the extremely high $H_2$ selectivity was achieved after aging.[22]

In this study, we elucidated the enhancement effect of long-term aging on the $H_2$-sensing performances of the sensor utilizing ZnO (+84 wt % $Ta_2O_5$)-SE. Specifically, we examined the changes in the morphology, crystal structure, and chemical surface state of the SE material after aging, including the corresponding changes in the catalytic activities.

## 2. EXPERIMENTAL SECTION

**2.1. Sensor Fabrication.** First, an intermediate YSZ layer (abbreviated as i-YSZ) between the SE layer and a YSZ tube (8 mol % $Y_2O_3$-doped $ZrO_2$, Nikkato, Japan) was formed; a YSZ powder (8 mol % $Y_2O_3$-doped $ZrO_2$, Tosoh, Japan) was mixed with $\alpha$-terpineol, and the resulting paste was applied to the surface of the YSZ tube. Utilization of such an additional YSZ layer between SE and a YSZ tube has been reported to facilitate the sensing-signal stabilization and to improve the mechanical stability of the SE/YSZ interface.[23] The physical dimensions of the hemispherically terminated tube utilized here were 300 mm in length and 5 and 8 mm in inner and outer diameters, respectively.

The SE paste was prepared by grinding a powdered ZnO (16 wt %; 99.99%, Kojundo Chemical, Japan) together with a powdered $Ta_2O_5$ (84 wt %; 99.99%, Kojundo Chemical, Japan) in a mortar and pestle, and then an organic binder ($\alpha$-terpineol) was added to the powder mixture. The obtained paste was applied to the surface of i-YSZ to form a 4-mm-wide banded SE layer. Platinum paste (Tanaka Kikinzoku, Japan) was applied on the inner-end surface of the YSZ tube, forming the reference electrode (RE). The painted YSZ tube was then dried at 130 °C and subsequently sintered at 1200 °C for 2 h in an air atmosphere.

**2.2. Sensing-Performance Evaluation.** The fabricated tubular YSZ-based sensors were assembled in a custom-made quartz testing cell in close proximity to a gas inlet and connected to a conventional gas-testing system equipped with a high-temperature electric furnace and a mass-flow controller system, as reported elsewhere.[20,21] Evaluation of the gas-sensing characteristics was performed at a constant operating temperature of 500 °C. The sensor was alternately exposed to the humidified base gas (21 vol % $O_2$ + 1.3 vol % $H_2O$ + $N_2$ balance) or the humidified sample gas containing $H_2$, CO, $C_3H_8$, $C_3H_6$, $CH_4$, $NH_3$, NO, or $NO_2$, diluted in the base gas with a total gas flow rate of 100 $cm^3$/min. The gas concentration of each sample gas was fixed at 100 ppm for cross-sensitivity measurements. The inner platinum electrode was always exposed to ambient air, functioning as a Pt/air-RE, while the SE was exposed to the sample or base gas. The difference in the potential (emf) between the SE connected to the positive terminal of an electrometer (R8240, Advantest, Japan) and the Pt/air-RE connected to the negative terminal was measured as a sensing signal. The gas sensitivity (Δemf) was defined as the difference between the emf value in the base gas and that in the sample gas.

**2.3. Polarization Curve Measurements.** The measurements of current−voltage (polarization) curves were conducted by means of an electrochemical analyzer (Autolab, PGSTAT30, Eco-Chemie, The Netherlands), based on a potentiodynamic method (at a constant scan rate of 8 mV/min), by using two electrode configurations in each of the base and sample gases (diluted with synthetic air or $N_2$). The modified cathodic polarization curve was obtained by plotting the absolute current value (measured in the base gas) against the applied potential. The modified polarization curves for the anodic reactions of each of the sample gases ($H_2$, $C_3H_6$, and CO, diluted with air) were obtained by subtracting the current value measured in the base gas from that in each sample gas (diluted with air). In the case of the anodic polarization curve measured in each of the sample gases ($H_2$, $C_3H_6$, and CO, diluted with $N_2$), the obtained anodic current value was plotted directly against the applied potential.

**2.4. X-ray Diffraction (XRD), Scanning Electron Microscopy (SEM), and X-ray Photoelectron Spectroscopy (XPS) Measurements.** The crystal structure change of the SE material before and after aging at 500 °C for 80 days was examined via an XRD analysis system (RINT 2100VLR/PC, Rigaku, Japan), with a Cu K$\alpha$ X-ray source ($\lambda$ = 1.5406 Å). To calibrate XRD patterns, an internal silicon reference powder (RSRP-43275G, Rigaku, Japan) was incorporated into the powder samples. The morphological change in the SE material before and after long-term aging was also observed by means of a field-emission scanning electron microscope (JSM-6340F, JEOL, Japan), operating at 5 kV. An XPS system (AXIS-165, Shimadzu/Kratos, Japan) was utilized for examination of the chemical surface state of the SE material before and after aging, by use of a monochromatic Al K$\alpha$ source for excitation (12 kV and 2 mA) under ultrahigh vacuum ($1.18 \times 10^{-6}$ Pa).

**2.5. Evaluation of the Gas-Phase Catalytic Activity.** Examination regarding the gas-phase catalytic activity of the SE material was conducted by using a cell arrangement similar to that reported elsewhere.[24] The SE-material powder (50 mg) was packed into a quartz tube, which was positioned inside a separate catalyst cell. This catalyst cell was located at the upstream of the sensing cell. The temperature inside the catalyst cell was maintained at the same temperature as that inside the sensing cell. The calibrated YSZ-based sensor using ZnO (+84 wt % $Ta_2O_5$)-SE was used to monitor the change in the $H_2$ concentration in the outlet gas from the catalyst cell, while an automotive emission analyzer (MEXA102G, Horiba, Japan) was utilized to monitor the change in the $C_3H_6$ concentration in the outlet gas.

All measurements stated in sections 2.4 and 2.5 were carried out by using ZnO (+84 wt % $Ta_2O_5$) as a powder sample rather than the fabricated electrode itself because of the incompatibility of the electrode for these techniques. Because the powder samples were fabricated and treated (aged) in the same manner as the SE was, they could be used as a substitute for the SE sample. Thus, we believe that the results obtained from either of the powder sample or the SE will not result in a significant difference.

## 3. RESULTS AND DISCUSSION

**3.1. Effect of Aging on the Electrode Composition and Morphology.** Initially, the sensor using ZnO (+84 wt % $Ta_2O_5$)-SE showed relatively sensitive and selective $H_2$ responses, as depicted in Figure 1a. The $H_2$ sensitivity was gradually increased and stabilized after aging for more than 40 days.[22] As shown in Figure 1b, the sensor became not only highly sensitive toward $H_2$ but also extremely selective to $H_2$ after long-term aging (for 80 days in this case). This significant change in the $H_2$ sensitivity after long-term aging was studied here by investigating the change in the crystal structure via XRD measurements and that in the morphology via SEM observations.

A comparison of the XRD patterns of the ZnO (+84 wt % $Ta_2O_5$) powder samples presented in Figure 2 shows a negligible change in the crystal structure of the initial state (before aging) sample (Figure 2a) and that of the sample aged at 500 °C for 80 days (Figure 2b). All of the XRD peaks in both

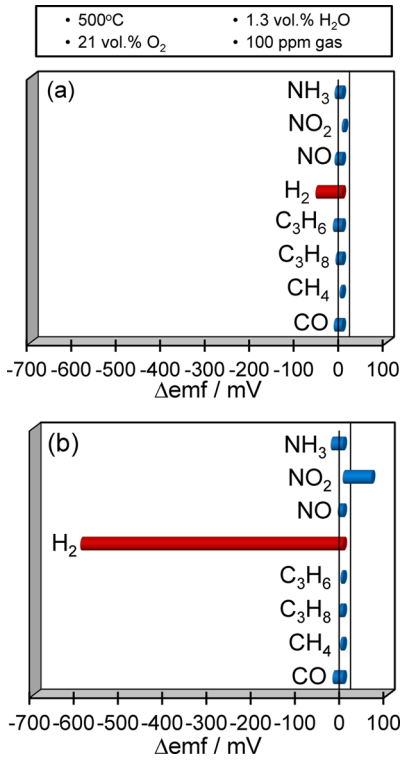


**Figure 1.** Cross-sensitivity of the sensor using ZnO (+84 wt % $Ta_2O_5$)-SE: (a) at the initial state; (b) at the stabilized state (after aging at 500 °C for 80 days) under humid conditions (1.3 vol % $H_2O$). Part a reprinted with permission from ref 21 and part b from ref 22. Copyright 2013 Elsevier.

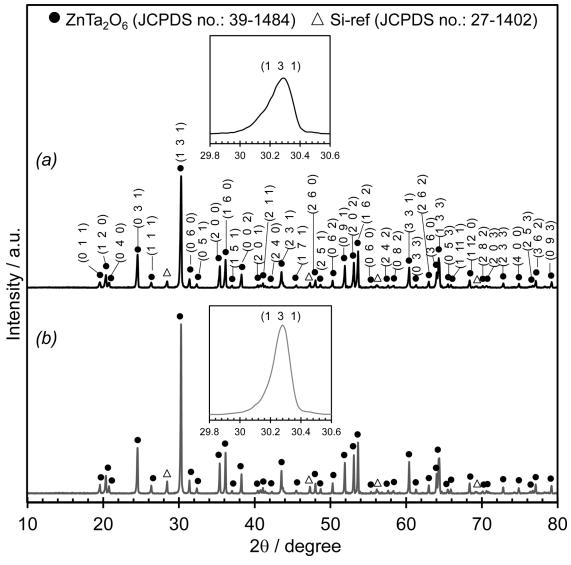


**Figure 2.** XRD patterns of the ZnO (+84 wt % $Ta_2O_5$) powder sample: (a) at the initial state; (b) after aging at 500 °C for 80 days. Inset: (131) peaks before and after aging.

samples were found to be in good agreement with those for $ZnTa_2O_6$ (JCPDS no. 39-1484). As can be seen from the respective insets in Figure 2, there is a subtle refinement in the peak shape to that of a singular reflection after aging, of (131) peaks compared before and after aging. This implies the presence of a small amount of another compound other than $ZnTa_2O_6$ at the bulk of the initial SE material.

The morphological change of the SE material due to aging was observed by means of SEM, and the results are presented in Figure 3. It is seen that the morphology of the ZnO (+84 wt

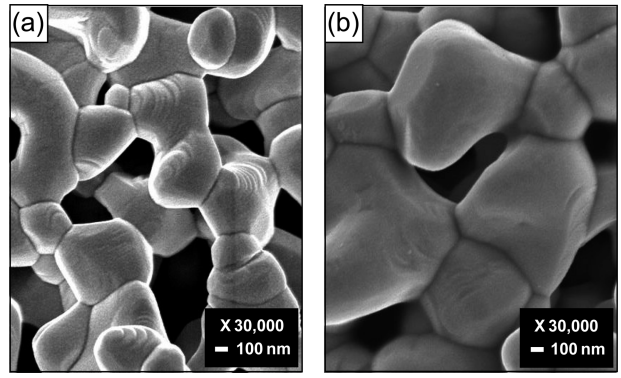


**Figure 3.** SEM images of the ZnO (+84 wt % $Ta_2O_5$) sample: (a) at the initial state; (b) after aging at 500 °C for 80 days.

% $Ta_2O_5$) powder sample just after sintering at 1200 °C for 2 h consists of polygonal-shaped particles with some stepped regions that appear on the surface of several particles (Figure 3a).

The particle size is in the range of 200 nm to 1.2 $\mu$m. Figure 3b shows the SEM image of the ZnO (+84 wt % $Ta_2O_5$)-SE sample after aging at 500 °C for 80 days. The particles enlarge and agglomerate after aging, with the particle size ranging from 500 nm to 1.4 $\mu$m. Additionally, the aging process also decreases the porosity of the SE material. A relatively denser morphology will naturally give a more tortuous diffusion path. Such a situation may be more favorable for a smaller molecular-sized gas such as $H_2$, to pass through the path, compared with larger molecular-sized gases. This may be one of the factors that result in a significant improvement of the $H_2$ selectivity after long-term aging of the sensor.

**3.2. Effect of Aging on the Chemical Surface State of SE.** A detailed study regarding the change in the chemical surface state of the SE materials before and after aging was performed via XPS measurements. The resulting spectra were treated by using a linear background and fitted with a Lorentzian−Gaussian function. Figure 4 shows a comparison of XPS spectra of Ta 4f, Zn 2p, and O 1s for the ZnO (+84 wt % $Ta_2O_5$) powder samples before and after aging for 80 days. The Ta 4f spectra of the initial state sample show a broad peak that can be deconvoluted and fitted into two doublets (Figure 4a and Table 1). The first pair of peaks is centered at ($4f_{7/2}$) 26.1 eV and ($4f_{5/2}$) 28.0 eV, with a spin−orbital splitting of 1.9 eV. The second set of peaks was found to consist of components that located at ($4f_{7/2}$) 27.0 eV and ($4f_{5/2}$) 28.9 eV, with an identical spin−orbital splitting of 1.9 eV. The observed binding-energy values are within the range of those reported for the oxidation (valence) state (5+) of tantalum.[25−28] This is consistent with the fact that tantalum exists as $Ta^{5+}$ in $ZnTa_2O_6$.

The two-doublet peaks observed here may be due to the following: the formation of a nonequilibrated Zn−Ta−O compound (like $Zn_3Ta_2O_8$) together with an equilibrated $ZnTa_2O_6$, particularly on the surface. The copresence of a surfacial compound like $Zn_3Ta_2O_8$ will very likely cause the appearance of another doublet because of the differing Ta−O bond lengths in $Zn_3Ta_2O_8$ (1.80 Å)[29] and $ZnTa_2O_6$ (1.93 Å).[30]

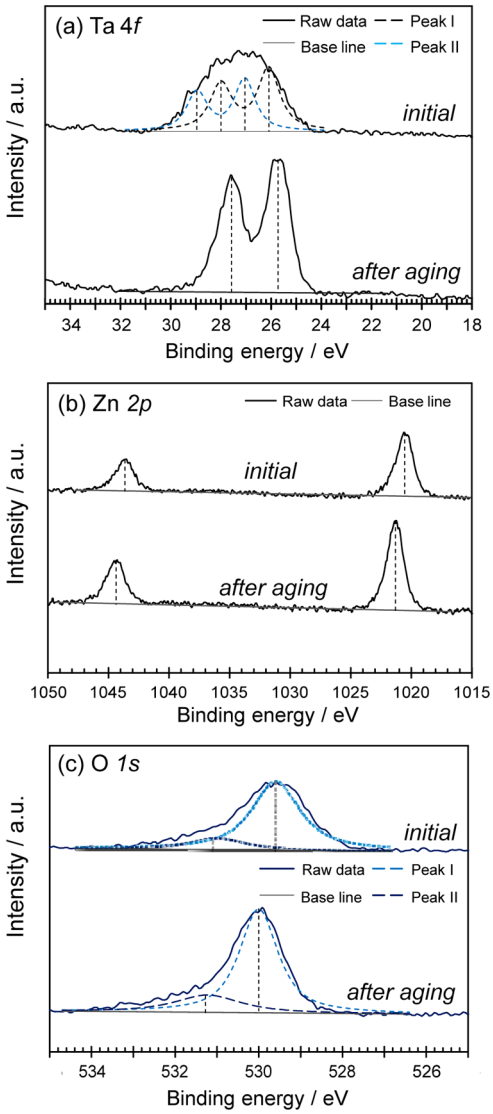


**Figure 4.** XPS spectra for (a) Ta 4f, (b) Zn 2p, and (c) O 1s of the ZnO (+84 wt % $Ta_2O_5$) powder samples at the initial state and after aging for 80 days.

**Table 1. Binding Energy of Ta 4f Peaks of the ZnO (+84 wt % $Ta_2O_5$) Powder Samples at the Initial State and after the Aging Process, in Comparison with the Commercial $Ta_2O_5$**

| | binding energy/eV | | |
|---|---|---|---|
| Ta 4f | initial state | after aging | commercial $Ta_2O_5$ |
| $4f_{7/2}$ | (i) 26.1 | 25.7 | 25.7 |
| | (ii) 27.0 | | |
| $4f_{5/2}$ | (i) 28.0 | 27.6 | 27.5 |
| | (ii) 28.9 | | |

The presence of another compound in the bulk was suggested in the previous XRD results, and then the XPS results here further confirmed the existence of a nonequilibrated compound, particularly concentrated on the surface.

After aging for 80 days, the broad spectrum (two-doublet) seen in the initial state sample was no longer observed, and it could be fitted into two peaks (one-doublet) centered at ($4f_{7/2}$) 25.7 eV and ($4f_{5/2}$) 27.6 eV, with a spin−orbital splitting of 1.9 eV (Figure 4a and Table 1). These peak values are consistent with the binding energy observed for the valence state (5+) of tantalum reported.[31−33] For the sake of comparison, an XPS measurement was carried out for a high-purity commercial $Ta_2O_5$ in which only $Ta^{5+}$ exists. As a result, the Ta 4f peaks at ($4f_{7/2}$) 25.7 eV and ($4f_{5/2}$) 27.5 eV observed for $Ta_2O_5$ are also in good agreement with those for the sample after aging, as given in Table 1. The similarity in the binding energy of Ta 4f between the aged sample and the reference $Ta_2O_5$ sample suggests that long-term aging at high temperature has possibly stabilized the chemical surface state of tantalum in the SE material of $ZnTa_2O_6$.

The effect of the aging process on the spectra of Zn 2p is depicted in Figure 4b. For the initial state sample, the Zn 2p spectra can be fitted into two components, centered at ($2p_{3/2}$) 1020.7 eV and ($2p_{1/2}$) 1043.7 eV, with a spin−orbital splitting of 23.0 eV. The binding-energy values observed here are similar to those reported for Zn 2p in ZnO.[34−36] After aging, the Zn 2p signal manifests as two components located at ($2p_{3/2}$) 1021.4 eV and ($2p_{1/2}$) 1044.4 eV. These binding-energy values are also in good agreement with that reported[37−39] for ZnO, where zinc exists as $Zn^{2+}$.

The O 1s spectra of both samples are given in Figure 4c, revealing a slight shift in the central binding energy from 529.6 to 530.0 eV after aging. The O 1s peak at this binding-energy value is in good agreement with those reported for Ta−O and Zn−O, whose binding energies are overlapping at approximately the same value.[32,35,39,40] Another smaller peak was also observed in both spectra at around 531.0 eV, which may be attributed to contamination of the surface hydroxyl group.[41,42]

It can be deduced from these results that initially both $ZnTa_2O_6$ and the nonequilibrated Zn−Ta−O compounds like $Zn_3Ta_2O_8$ exist on the surface of the SE. The aging process is postulated to stabilize the nonequilibrated compound, resulting in a large change in the binding energy of Ta 4f. The change in the Ta 4f spectra is accompanied by a shift in the binding energy of Zn 2p and O 1s. Such a stabilization may result in a change in the catalytic activities against key reactions that govern sensing-signal generation. Because there are several reactions (i.e., electrochemical and gas phase) affecting generation of the sensing signal, the next investigations should be carried out with aspiration of determining which reaction would be most affected.

**3.3. Effect of Aging on the Catalytic Activity.** The sensing mechanism of the developed sensor has been confirmed to be based on the mixed-potential model.[22] When the SE of a mixed-potential-type sensor is exposed to the sample gas diluted with air, a mixed potential can be established when the cathodic (eq 1) and anodic (represented by eq 2 in the case of $H_2$ sensing) reactions occur at the same rate at the interface of YSZ/SE.

$$2O_2 + 4e^- \rightarrow 2O^{2-} \quad (1)$$

$$2H_2 + 2O^{2-} \rightarrow 2H_2O + 4e^- \quad (2)$$

However, prior to the proceeding electrochemical reactions at the YSZ/SE interface, the sample gas will be naturally oxidized within the SE layer by heterogeneous catalysis. Hence, the reactivity to the gas-phase reaction (represented by eq 3 in the case of $H_2$ sensing) can control the number of gas species capable of reaching the YSZ/SE interface.

$$2H_2(g) + O_2(g) \rightarrow 2H_2O(g) \quad (3)$$

The mixed-potential model can be commonly rationalized by using polarization curves (Scheme 1a), where the intersect

**Scheme 1. Illustration of the Mixed-Potential Model by Using (a) Standard Modified Polarization Curves and the Explanation of the Drastic Change in the Gas Sensitivity of the Developed Sensor (b) at the Initial State and (c) after Aging**

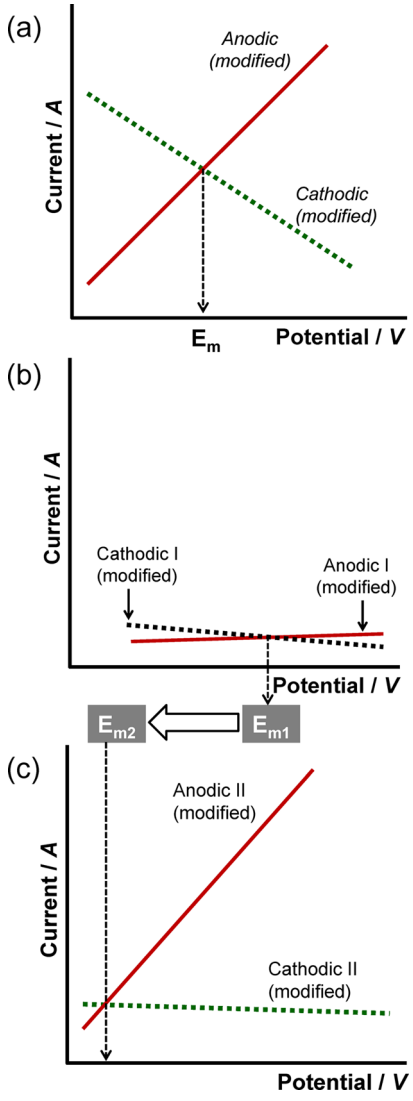


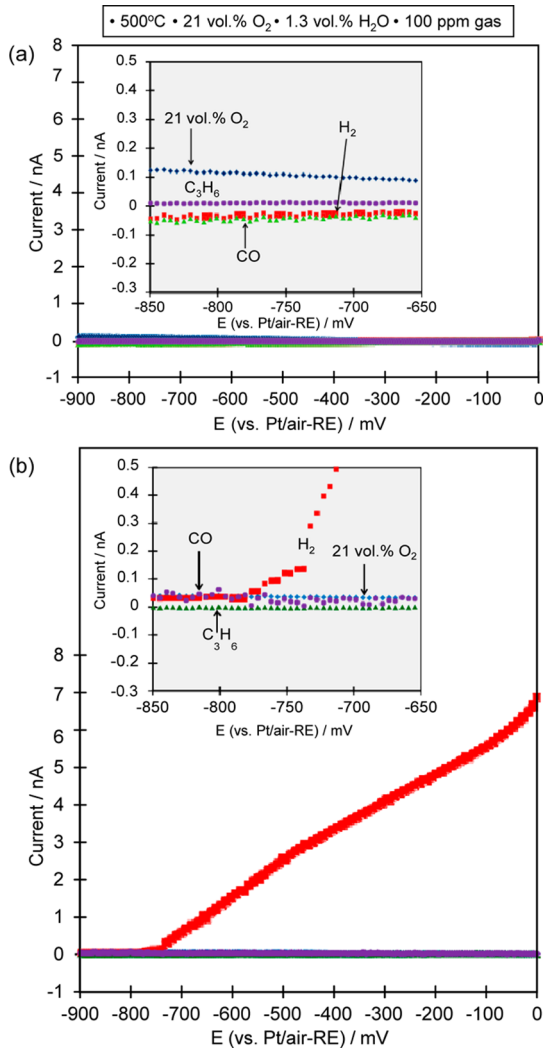


**Figure 5.** Modified polarization curves for the anodic reaction of each sample gas ($H_2$, $C_3H_6$, and CO, 100 ppm each) and for the cathodic reaction of 21 vol % $O_2$ for the sensor using ZnO (+84 wt % $Ta_2O_5$)-SE: (a) at the initial state; (b) after aging for 80 days. Insets: enlarged figures especially in the potential range from −850 to −650 mV (vs Pt/air-RE).

point of the modified anodic and cathodic polarization curves is assigned as the mixed potential ($E_m$). Therefore, in this study, the changes in the catalytic activities against the gas-phase and/or electrochemical reactions before and after long-term aging were elucidated by measurements of the polarization curves as well as gas-phase catalytic activities.

Initially, the polarization-curve measurements were carried out in the sample gas [$H_2$, $C_3H_6$, and CO, diluted with air (21 vol % $O_2$)]. When the measurements are conducted in an oxygenated atmosphere, the heterogeneous catalysis that usually occurs within the SE layer will deplete the fraction of available sample-gas molecules. Then, the unreacted sample-gas molecules can reach TPB and undergo electrochemical reactions there. As can be seen from Figure 5, the generated cathodic current values measured in air (21 vol % $O_2$) are very low (<0.1 nA in the examined potential range) for the sensor using ZnO (+84 wt % $Ta_2O_5$)-SE, both before and after aging for 80 days. The generated current for the anodic reaction of $H_2$ increased significantly after aging in the potential range starting from around −750 mV (vs Pt/air-RE), while those of $C_3H_6$ and CO were unaffected by aging.

Before aging, the combination of the low cathodic current of $O_2$ and the low anodic current of the sample gas will result in low mixed potential (as depicted in Scheme 1b). This was experimentally confirmed to result in low sensitivities for $H_2$, $C_3H_6$, and CO (Figure 1a). After aging, a significant increase in the anodic current of $H_2$ shifted the mixed potential to a more negative direction (Figure 5b and Scheme 1c), which manifested experimentally as the higher $H_2$ sensitivity (Figure 1a). However, because such a drastic increase in the anodic current of $H_2$ was not observed in the cases of $C_3H_6$ and CO (Figure 5b), the sensitivities to these gases after aging remained low (Figure 1b).

From the perspective of a mixed-potential model, the increase in the rate of the anodic reaction of $H_2$ after long-term aging may arise from either an increase in the catalytic activity to the anodic reaction of $H_2$ and/or a decrease in heterogeneous catalysis to the gas-phase reaction of $H_2$. To confirm further the change in the catalytic activity toward the


dx.doi.org/10.1021/am403952w | ACS Appl. Mater. Interfaces 2013, 5, 12099−12106

anodic reactions of each sample gas ($H_2$, $C_3H_6$, and CO) before and after aging, additional polarization-curve measurements were then conducted in the absence of $O_2$ (in $N_2$). Because heterogeneous catalysis is considered to be negligible under this set of conditions, all of the sample gases passing through the SE layer can reach TPB and electrochemically react with $O^{2-}$ .

Figure 6 shows a comparison of the polarization curves measured in each sample gas ($H_2$, $C_3H_6$, and CO) in the

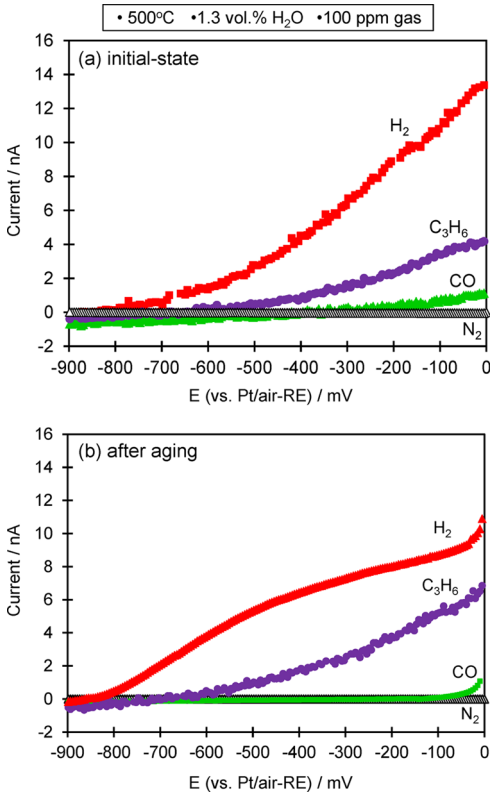


**Figure 6.** Polarization curves measured in each sample gas ($H_2$, $C_3H_6$, and CO, 100 ppm each, diluted with $N_2$) for the sensor using ZnO (+84 wt % $Ta_2O_5$)-SE: (a) at the initial state; (b) after aging for 80 days.

absence of $O_2$ for the sensor using ZnO (+84 wt % $Ta_2O_5$)-SE before and after aging for 80 days. It is seen from Figure 6a that the anodic current values of each sample gas were rather high even before aging compared with those measured in the presence of $O_2$ (Figure 5a). It is also clear that the anodic current value of $H_2$ is relatively higher than those of $C_3H_6$ and CO both before and after aging (Figure 6a,b). In addition, it is noted that the shapes of the anodic polarization curves measured in each sample gas did not significantly change after aging (Figure 6a,b). These results suggest that the catalytic activity toward the anodic reactions of each sample gas is also not changed largely before and after aging. However, the catalytic activity to the anodic reaction of $H_2$ remains comparatively higher than those of $C_3H_6$ and CO. Through a comparison of these polarization curves (Figure 6) with those measured in each sample gas diluted with air (Figure 5), it is can be concluded that the heterogeneous catalytic activity to the gas-phase reaction only to $H_2$ is significantly different between the initial and aged samples, while those of $C_3H_6$ and CO remain high even after the aging process. This, in turn, results in low sensitivities to $C_3H_6$ and CO, which brings about a highly selective response toward $H_2$, accompanied with high $H_2$ sensitivity.

In order to confirm this assumption, conversion of the sample gas ($H_2$ or $C_3H_6$, diluted with air) in the gas-phase oxidation was evaluated. As shown in Figure 7, the initial state

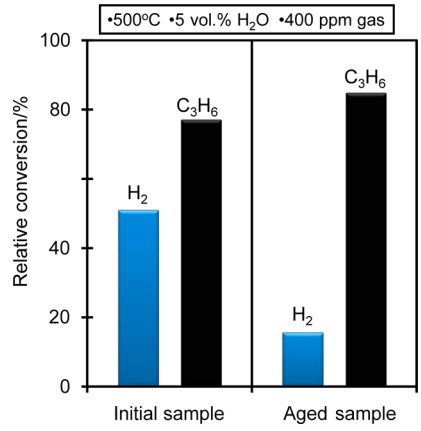


**Figure 7.** Comparison of the conversion of $H_2$ and $C_3H_6$ in gas-phase oxidation on each of the initial and aged ZnO (+84 wt % $Ta_2O_5$) powder samples.

of the ZnO (+84 wt % $Ta_2O_5$) powder sample gave higher catalytic activity to the gas-phase oxidation of $H_2$ when compared with the aged sample; conversion of $H_2$ decreased significantly from 50% to 15%, as expected. In contrast, $C_3H_6$ conversion showed only a minor difference between the initial and aged samples. This indicates that the high catalytic activity toward the gas-phase reaction of $H_2$ is significantly decreased by aging, while that of $C_3H_6$ is evidently unaffected.

**3.4. Aging Mechanism in Enhancing the Sensitivity and Selectivity against $H_2$.** The aging effects on the sensing performances and the SE material properties are summarized in Table 2 and Scheme 2. In Scheme 2, a thicker arrow indicates a higher gas fraction and a thinner arrow indicates a lower gas fraction. The initial-state morphology of $ZnTa_2O_6$-SE was confirmed to be rather porous with smaller-sized particles. The broad Ta 4f spectra observed for the initial-state SE material suggests the existence of a nonequilibrated Zn−Ta−O compound (like $Zn_3Ta_2O_8$) together with pure $ZnTa_2O_6$, particularly on the surface of the SE material. This initial-state SE material possesses high catalytic activity to both the gas-phase and anodic reactions of the sample gases (such as $H_2$, $C_3H_6$, and CO). High catalytic activity to the gas-phase reaction reduces the number of gases capable of reaching the SE/YSZ interface, as depicted in Scheme 2a. However, because the reactivity to the anodic reaction of $H_2$ is higher than those for CO and $C_3H_6$, a relatively sensitive and selective response toward $H_2$ was observed at the initial state (before aging).

After a stabilized state was attained by long-term aging, the SE was comprised of larger particles with relatively lower porosity. A significant change was observed for the chemical surface state of the aged SE material. Long-term aging has presumably stabilized the surficial nonequilibrated Zn−Ta−O compound (like $Zn_3Ta_2O_8$) into a very stable form, resulting in transformation of the Ta 4f broad peak (two-doublet) into a one-doublet peak with lower binding-energy values. This stabilized (aged) SE material has been proven to have a significantly lower catalytic activity to heterogeneous oxidation of $H_2$, allowing a higher fraction of $H_2$ to reach the TPB, as

Table 2. Summary of the Aging Effect on Various and Sensing Properties of the ZnO (+84 wt % $Ta_2O_5$)-SE Material

| SE condition | main SE component (bulk) | particle size | XPS spectra (Ta 4f) | catalytic properties: sample gas | gas-phase (heterogeneous) | anodic reaction in the sample gas | cathodic reaction of $O_2$ | gas sensitivity | gas selectivity |
|---|---|---|---|---|---|---|---|---|---|
| initial state | $ZnTa_2O_6$ | smaller | two- doublet (in higher binding energy) | $H_2$ | high | high | low | low | moderate |
| | | | | $C_3H_6$ | high | moderate | | low | low |
| | | | | CO | high | lower | | low | low |
| after aging | $ZnTa_2O_6$ | larger | one- doublet (in lower binding energy) | $H_2$ | **low** | high | low | **high** | **high** |
| | | | | $C_3H_6$ | high | moderate | | low | low |
| | | | | CO | high | lower | | low | low |

Scheme 2. Illustration of the Aging Effect on Enhancement of the Sensing Performance of the Sensor Using ZnO (+84 wt % $Ta_2O_5$)-SE (a) at the Initial State and (b) after Aging

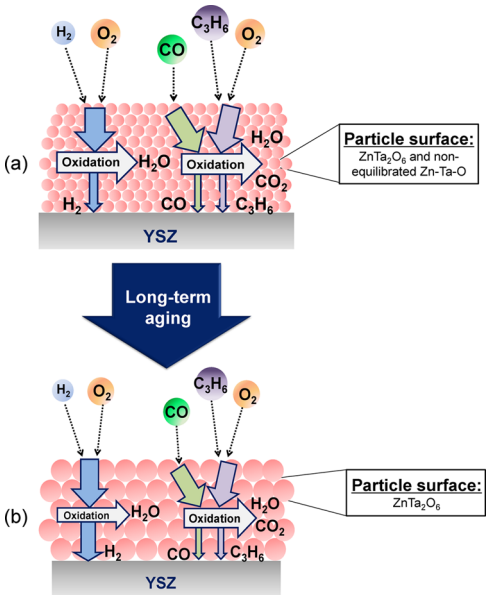


shown in Scheme 2b. However, because the catalytic activity to the heterogeneous oxidation of $C_3H_6$ (or CO) is still high, the fraction of $C_3H_6$ (or CO) that reaches the TPB remains low.

Despite this, the catalytic activity to the anodic reaction of the sample gases ($H_2$, CO, and $C_3H_6$) was not affected by aging. Therefore, a higher fraction of $H_2$ can react with $O^{2-}$ at TPB and result in a significant increase in the $H_2$ sensitivity, while maintaining a lower sensitivity to CO and $C_3H_6$.

The fact that the catalytic activity toward the anodic reaction of the sample gases ($H_2$, CO, and $C_3H_6$) remains unchanged after long-term aging suggests that the active sites for the anodic reaction of these gases are hardly affected by the aging process. On the contrary, the stabilization process during aging evidently reduced the number of active sites especially for heterogeneous catalysis of $H_2$ oxidation, while those for CO and $C_3H_6$ seem to be less affected. The major changes in the XPS spectra of Ta 4f after aging appear to strongly correlate with transformation of the initial nonequilibrated surface compound to a fully equilibrated one. The presence of the nonequilibrated phase at the initial state is believed to possess a comparatively greater number of active sites for heterogeneous catalysis, facilitating higher rates of $H_2$ oxidation. This contributed to the higher observed augmentation in both the sensitivity and selectivity toward $H_2$ after aging. However, the reason why only the active site for heterogeneous $H_2$ oxidation is affected by the aging process warrants further investigation.

## 4. CONCLUSIONS

The effects of long-term aging on various properties of the SE material have been investigated and characterized for the sensor using ZnO (+84 wt % $Ta_2O_5$)-SE. The XRD patterns of the SE material before and after aging for 80 days confirmed the presence of $ZnTa_2O_6$ as the main SE component in the bulk of both samples. The aging process was found to promote particle agglomeration, as suggested by a change in the particle size observed in SEM images of the aged sample. The initial-state sample (before aging) having overlapping Ta 4f peaks may be indicative of the copresence of the nonequilibrated surficial Zn−Ta−O compound (like $Zn_3Ta_2O_8$) together with stable pure $ZnTa_2O_6$. The initial-state sample was confirmed to have high catalytic activities against the gas-phase (heterogeneous) reactions as well as the anodic reactions toward each sample gas ($H_2$, CO, and $C_3H_6$), resulting in lower sensitivity and moderate selectivity to $H_2$. During the aging process, the nonequilibrated Zn−Ta−O compound existing on the surface of the SE material was stabilized and converted to an equilibrated compound (pure $ZnTa_2O_6$), as suggested by the well-defined valence state of Ta 4f, which was in good agreement with the $Ta^{5+}$ oxidation state. The stabilized SE material was found to have a lower catalytic activity to the heterogeneous oxidation of $H_2$, and it maintained a preferential catalytic activity to the anodic reaction of $H_2$ compared with those for CO and $C_3H_6$. This caused the developed sensor to become highly sensitive and highly selective toward $H_2$ after long-term aging. Future investigation will be focused on further reducing the stabilization time.

## AUTHOR INFORMATION

### Corresponding Author

*Tel: +81-92-583-8852. Fax: +81-92-583-8976. E-mail: miurano@astec.kyushu-u.ac.jp.

### Author Contributions

[§]This work was partly conducted under previous appointment as a JSPS postdoctoral fellow.

### Notes

The authors declare no competing financial interest.

## ACKNOWLEDGMENTS

This work was supported by JSPS KAKENHI Grants 22350095 and 25288109. The authors also gratefully acknowledge the Center of Advanced Instrumental Analysis in Kyushu University for providing assistance with the XPS measurements.

## REFERENCES


(1) Yu, S.; Wu, Q.; Tabib-Azar, M.; Liu, C. *Sens. Actuators, B* **2002**, *85* (3), 212−218.
(2) Park, C. O.; Fergus, J. W.; Miura, N.; Park, J. *Ionics* **2009**, *15* (3), 261−284.
(3) Ramamoorthy, R.; Dutta, P. K.; Akbar, S. A. *J. Mater. Sci.* **2003**, *38* (21), 4271−4282.
(4) Miura, N.; Elumalai, P.; Plashnitsa, V. V.; Ueda, T.; Wama, R.; Utiyama, M. In *Solid State Gas Sensing*; Comini, E., Faglia, G., Sberveglieri, G., Eds.; Springer Science + Business Media, LLC: Berlin, 2009; p 182.
(5) Elumalai, P.; Plashnitsa, V. V.; Ueda, T.; Hasei, M.; Miura, N. *Ionics* **2006**, *12* (6), 331−337.
(6) Plashnitsa, V. V.; Ueda, T.; Elumalai, P.; Miura, N. *Sens. Actuators, B* **2008**, *130* (1), 231−239.
(7) Sekhar, P. K.; Brosha, E. L.; Mukundan, R.; Li, W.; Nelson, M. A.; Palanisamy, P.; Garzon, F. H. *Sens. Actuators, B* **2010**, *144* (1), 112−119.
(8) Sekhar, P. K.; Brosha, E. L.; Mukundan, R.; Nelson, M. A.; Toracco, D.; Garzon, F. H. *Solid State Ionics* **2010**, *181* (19−20), 947−953.
(9) Yamaguchi, M.; Anggraini, S. A.; Fujio, Y.; Breedon, M.; Plashnitsa, V. V.; Miura, N. *Electrochim. Acta* **2012**, *76*, 152−158.
(10) Anggraini, S. A.; Breedon, M.; Miura, N. *J. Electrochem. Soc.* **2013**, *160* (9), B164−B169.
(11) Park, J.; Yoon, B. Y.; Park, C. O.; Lee, W.; Lee, C. B. *Sens. Actuators, B* **2009**, *135* (2), 516−523.
(12) Mukundan, R.; Brosha, E. L.; Brown, D. R.; Garzon, F. H. *J. Electrochem. Soc.* **2000**, *147* (4), 1583−1588.
(13) Lu, G.; Miura, N.; Yamazoe, N. *J. Mater. Chem.* **1997**, *7*, 1445−1449.
(14) Miura, N.; Wang, J.; Nakatou, M.; Elumalai, P.; Zhuiykov, S.; Hasei, M. *Sens. Actuators, B* **2006**, *114* (2), 903−909.
(15) Zosel, J.; Westphal, D.; Jakobs, S.; Müller, R.; Guth, U. *Solid State Ionics* **2002**, *152*−*153*, 525−529.
(16) Szabo, N. F.; Dutta, P. K. *Solid State Ionics* **2004**, *171* (3−4), 183−190.
(17) Elumalai, P.; Wang, J.; Zhuiykov, S.; Terada, D.; Hasei, M.; Miura, N. *J. Electrochem. Soc.* **2005**, *152* (7), H95−H101.
(18) Hibino, T.; Kakimoto, S.; Sano, M. *J. Electrochem. Soc.* **1999**, *146* (9), 3361−3366.
(19) Mukundan, R.; Brosha, E. L.; Garzon, F. H. *J. Electrochem. Soc.* **2003**, *150* (12), H279−H284.
(20) Plashnitsa, V. V.; Elumalai, P.; Kawaguchi, T.; Fujio, Y.; Miura, N. *J. Phys. Chem. C* **2009**, *113* (18), 7857−7862.
(21) Anggraini, S. A.; Breedon, M.; Miura, N. *Sens. Actuators, B* **2013**, *187*, 58−64.
(22) Anggraini, S. A.; Breedon, M.; Miura, N. *Electrochem. Commun.* **2013**, *31*, 133−136.
(23) Fujio, Y.; Plashnitsa, V. V.; Elumalai, P.; Miura, N. *Talanta* **2011**, *85* (1), 575−581.
(24) Yamaguchi, M.; Anggraini, S. A.; Fujio, Y.; Sato, T.; Breedon, M.; Miura, N. *Int. J. Hydrogen Energy* **2013**, *38* (1), 305−312.
(25) Mahmood, K.; Park, S. B.; Sung, H. J. *ACS Appl. Mater. Interfaces* **2013**, *5* (9), 3722−3730.
(26) Basame, S. B.; White, H. *Langmuir* **1999**, *15* (3), 819−825.
(27) Skadtchenko, B. O.; Trudeau, M.; Kwon, C.; Dunn, B.; Antonelli, D. *Chem. Mater.* **2004**, *16* (15), 2886−2894.
(28) Xu, C.; Xiao, Q.; Ma, J.; Jin, Y.; Shao, J.; Fan, Z. *Appl. Surf. Sci.* **2008**, *254* (20), 6554−6559.
(29) Waburg, M.; Müller-Buschbaum, H. *Monatsh. Chem.* **1984**, *115*, 15−20.
(30) Waburg, M.; Müller-Buschbaum, H. *Z. Anorg. Allg. Chem.* **1984**, *508*, 55−60.
(31) Tüysüz, H.; Chan, C. K. *Nano Energy* **2013**, *2* (1), 116−123.
(32) Wei, A. X.; Ge, Z. X.; Zhao, X. H.; Liu, J.; Zhao, Y. *J. Alloys Compd.* **2011**, *509* (41), 9758−9763.
(33) Wang, N.; Li, H.; Wang, J.; Chen, S.; Ma, Y.; Zhang, X. *ACS Appl. Mater. Interfaces* **2012**, *4* (9), 4516−4523.
(34) Wang, J.; Tsuzuki, T.; Tang, B.; Hou, X.; Sun, L.; Wang, X. *ACS Appl. Mater. Interfaces* **2012**, *4* (6), 3084−3090.
(35) Deng, X.; Yao, K.; Sun, K.; Li, W.; Lee, J.; Matranga, C. *J. Phys. Chem. C* **2013**, *117* (21), 11211−11218.
(36) Agrell, J.; Boutonnet, M.; Melian-Cabrera, I.; Fierro, J. L. G. *Appl. Catal., A* **2003**, *253* (1), 201−211.
(37) Zheng, Y.; Zheng, L.; Zhan, Y.; Lin, X.; Zheng, Q.; Wei, K. *Inorg. Chem.* **2007**, *46* (17), 6980−6986.
(38) Chen, C.; He, H.; Lu, Y.; Wu, K.; Ye, Z. *ACS Appl. Mater. Interfaces* **2013**, *5* (13), 6354−6359.
(39) De la Rosa, E.; Sepulveda-Guzman, S.; Reeja-Jayan, B.; Torres, A.; Salas, P.; Elizondo, N.; Yacaman, M. J. *J. Phys. Chem. C* **2007**, *111* (24), 8489−8495.
(40) Wu, S. J.; Houng, B.; Huang, B. *J. Alloys Compd.* **2009**, *475* (1−2), 488−493.
(41) Karamat, S.; Rawat, R. S.; Lee, P.; Tan, T. L.; Ramanujan, R. V.; Zhou, W. *Appl. Surf. Sci.* **2010**, *256* (8), 2309−2314.
(42) Wang, J.; Xu, M.; Zhao, R.; Chen, G. *Analyst* **2010**, *135* (8), 1992−1996.